Neural Network Detection and Segmentation of Mental Foramen in Panoramic Imaging

Lazar Kats* / MarilenaVered*,**/ Sigalit Blumer ***/ Eytan Kats****

Objective: *To apply the technique of deep learning on a small dataset of panoramic images for the detection and segmentation of the mental foramen (MF).* ***Study design:*** *In this study we used in-house dataset created within the School of Dental Medicine, Tel Aviv University. The dataset contained randomly chosen and anonymized 112 digital panoramic X-ray images and corresponding segmentations of MF. In order to solve the task of segmentation of the MF we used a single fully convolution neural network, that was based on U-net as well as acascade architecture. 70% of the data were randomly chosen for training, 15% for validation and accuracy was tested on 15%. The model was trained using NVIDIA GeForce GTX 1080 GPU. The SPSS software, version 17.0 (Chicago, IL, USA) was used for the statistical analysis. The study was approved by the ethical committee of Tel Aviv University.* ***Results:*** *The best results of the dice similarity coefficient (DSC), precision, recall, MF-wise true positive rate (MF_{TPR}) and MF-wise false positive rate (MF_{FPR}) in single networks were 49.51%, 71.13%, 68.24%, 87.81% and 14.08%, respectively. The cascade of networks has shown better results than simple networks in recall and MF_{TPR}, which were 88.83%, 93.75%, respectively, while DSC and precision achieved the lowest values, 31.77% and 23.92%, respectively.* ***Conclusions:*** *Currently, the U-net, one of the most used neural network architectures for biomedical application, was effectively used in this study. Methods based on deep learning are extremely important for automatic detection and segmentation in radiology and require further development.*

Keywords: *neural network, mental foramen, panoramic imaging, detection, segmentation*

INTRODUCTION

The mental foramen (MF) is an important anatomical and clinical landmark for a range of dental procedures, from injections for local anesthesia to maxillofacial and plastic surgery. The MF is located on the buccal surface of the mandible cortex and the mental nerve, the final branch of the inferior alveolar nerve, and associated blood vessels pass through it [1]. Complications in this area after different dental treatments can result in hematomas, anesthetic toxicity and various neurosensory disturbances [2-4]. It should be noted that long-term sequela of extractions in the area of the MF can lead to bone atrophy with a superficial position of the nerve, ultimately resulting in neurosensory impairments and compromised dental rehabilitation.

There is a significant anatomical variability in the location, number, radiological density and shape of the MF [5]. MF is located approximately halfway across the alveolar crest to the inferior border of the mandible in the area between the mesial apex of the first premolar to the mesial apex of the first molar roots. The MF shape can be round, oblong, linear or slit-shaped, with regular or irregular boundaries and partial or full cortication. In about 0.7 % to 12.5% there may be an additional MF that is equally important for dental treatments [6-8]. Noteworthy are those cases where the projection of the MF overlaps over the adjacent tooth root apex,

* Lazar Kats, DMD, Department of Oral Pathology, Oral Medicine and Maxillofacial Imaging, School of Dental Medicine, Tel Aviv University, Tel Aviv, Israel.
**: MarilenaVered, DMD, Institute of Pathology, The Chaim Sheba Medical Center, Tel Hashomer, Ramat Gan, Israel.
***: Sigalit Blumer, DMD, Department of Pediatric Dentistry, School of Dental Medicine, Tel Aviv University, Tel Aviv, Israel.
****: Eytan Kats, BSc, Freelance algorithm developer, Haifa, Israel.

Send all correspondence to:
Lazar Kats
Department of Oral Pathology, Oral Medicine and Maxillofacial Imaging
School of Dental Medicine
Tel Aviv University
Tel Aviv 69978
Israel
Phone: +972-3-6409305
Fax: +972-3-6409250
E-mail: lazarkat@tauex.tau.ac.il

therefore resembling different periapical pathologies, ranging from inflammatory granulomas to neoplasms.

Usually, the MF is well visualized in three-dimensional images like computed tomography (CT) and cone-beam (CB)-CT [7], however, on clinical grounds, two-dimensional images are the primary or only available images [8]. The most common extraoral two-dimensional image in dentistry is the panoramic image. It is impossible to determine the MF on several types of images, and in many instances, the detection of the foramen and its boundaries is challenging. Thus, the high variability in anatomical position and shape, as well as the partial information provided by two-dimensional images, makes it very difficult to detect this important formation, which is of particular importance for surgical interventions [9, 10].

Recently, there has been a great focus on the effectiveness of computer-aided diagnostics for the detection of anatomical formations and pathologies in medical radiology. Most methods use deep learning based on neural networks for this purpose. In line with this, progress has been made, at least at the research level, in the analysis of images of the brain [11], lungs [12] and breast[13]. Neural networks have been used to identify different details in these images using algorithms for classification, object detection and segmentation. Among these algorithms, the most difficult task is segmentation, as in addition to the detection of the object there is a need to define and mark its boundaries.

In the field of oral and maxillofacial radiology, a number of studies have been performed, including automatic detection and classification of teeth [14-17], detection of dental caries [18], periodontal evaluation [19, 20], detection of manifestations in jaws of systemic conditions as osteoporosis [21] and atherosclerotic carotid plaques [22], prediction of the occurrence of bisphosphonate-related osteonecrosis of the jaw [23], detection of maxillary sinusitis [24], temporomandibular joint damaged by osteoarthritis [25, 26], and even detection of various lesions (i.e., inflammatory cysts, tumors) [27-30]. It should be emphasized that most studies of this kind require the use of large datasets of images. In dentistry, this is a very difficult task, associated with the integration of a large number of varied clinics and X-ray services. In this study, we have tried to use a small dataset of panoramic images with a neural network architecture suitable for this purpose.

Thus, the objective of this study was to apply the technique of deep learning based on neural networks on a small dataset of panoramic images for the detection and segmentation of the MF.

MATERIALS AND METHOD

Network Architecture

In order to solve the task of segmentation of the mental foramen (MF) we used single fully convolution neural network, that was based on U-net [31] as well as a cascade architecture.

Single network

Similar to the U-net, neural network is divided into two pathways. A contracting path alternates 3x3 convolution layers and 2x2 max-pooling layers with stride 2 for down-sampling, an expansive path, alternates 3x3 convolution layers and 2x2 transposed convolution layers as proposed by Brosch *et al* [32]. Shortcut connections are used between corresponding layers of the two paths to leverage both high- and low-level features. All convolution layers, except the last, are followed by rectified linear units (ReLU) [33]. Activations of the last convolution layer are fed to the sigmoid function, that produces probabilistic segmentation map with values in the range between 0 and 1. To produce a final binary mask from the probabilistic output of the model, we applied a fixed threshold, that maximizes the mean dice similarity coefficient [34] over the training set. In addition, the Tversky index [35] was used as an objective function to tune the balance between precision and recall by changing the hyperparameter α.

Cross Validation

In order to get more confidence results on a small dataset we applied a 5-fold cross-validation method. The original dataset was randomly partitioned into 5 equal size subsamples. A single subsample was retained as the test data, and the remaining 4 subsamples were used as the training data. The process was repeated 5 times, with each of the 5 subsamples being used exactly once as the test data. The results from the experiments were averaged to produce a single estimation.

Cascade of networks

In order to achieve a better balance between precision and recall as well as between MF-wise true positive rate and MF-wise false positive rate, we trained the cascade model. Each network in the cascade was trained separately, when α value of the objective function is increasing from the first network in the cascade to the last one. Probabilistic segmentation maps of first and second networks in cascade were fed as additional input channel to second and third networks, accordingly. We used α equals to 0.01, 0.1 and 0.5 for the first, second and third network in the cascade, accordingly.

Dataset

In this study we used in-house dataset created within the School of Dental Medicine, Tel Aviv University. The study was approved by the ethical committee of Tel Aviv University. The dataset contained randomly chosen and anonymized 112 digital Panoramic x-ray images from CS 8100 Digital Panoramic System (Carestream Dental LLC, Atlanta, USA) and corresponding segmentations of MF (Fig. 1). Selection and segmentation were made by specialists in oral medicine with special training in oral and maxillofacial radiology. After the primary segmentation, all pictures were re-evaluated for the accuracy of segmentation. This data is challenging due to the large variability in MF size, shape, intensity as well as varying contrasts and sharpness of images produced by different devices.

X-Ray images were resized to 512x1024 pixels. Fig. 1 shows the original digital panoramic x-ray image (Fig. 1(a)) and corresponding manual segmentation of the MF (Fig. 1(b)). From each image we automatically cropped left (Fig. 1(c)) and right (Fig. 1(e)) region of interest (ROI) and generated segmentation mask (Fig. 1(d, f)), when boundaries of ROI are the same for all images and calculated from the training data based on location of MF. As there was a small amount of available training data, we used data augmentation by randomly flipping and rotating cropped ROIs to multiple angles. This allowed the network to learn from larger variability of examples and prevented overfitting.

Training Details

The input images and their corresponding segmentation maps were used to train the network in the mini-batch manner, when batch size was set to 32. Gradient descent computation and updates were carried out by Adam optimizer with fixed learning rate 0.001. Objective function is defined as minus Tversky index. For the implementation, we used Keras with Tensorflow backend. In this way, 70% of the data were randomly chosen for training, 15% for validation and accuracy was tested on 15%. The model was trained using NVIDIA GeForce GTX 1080 GPU.

Metrics for Statistical analysis

We used the following measures to produce a comprehensive evaluation of segmentation accuracy:

- Dice similarity coefficient (DSC): to compute a normalized overlap value between the produced and ground truth segmentations
- Precision (positive predictive rate): to express the proportion between the true segmented pixels and all pixels in our model associated with MF
- Recall (sensitivity): to express the proportion between the true segmented pixels and all MF pixels
- MF-wise true positive rate (MF_{TPR}): to express the proportion between the true detected MF and all MF in ground truth segmentations. The segmented area is considered as MF if the area size is not less than minimum size of the single MF in the dataset that was established as 8 pixels.
- MF-wise false positive rate (MF_{FPR}): to express the proportion between the false detected MF and number of all MF in produced segmentations.

The SPSS software, version 17.0 (Chicago, IL, USA) was used for the statistical analysis.

RESULTS

We explored the effect of different α values of the Tversky index by training the single networks model for each value separately and summarized the results in Table 1. In addition, a comparison with the cascade of networks was performed. With the decrease in the Tversky index there were no significant changes in the DSC, marked by an increase in recall, MF_{TPR} and MF_{FPR}, as well as a decrease in precision. The best results of the DSC, precision, recall, MF_{TPR} and MF_{FPR} in single networks were 49.51%, 71.13%, 68.24%, 87.81% and 14.08%, respectively. The cascade of networks has shown better results than simple networks in recall and MF_{TPR}, which were 88.83% and 93.75%, respectively, while DSC and precision had the lowest values, 31.77% and 23.92%, respectively.

Despite the models testing in a wide range of segmentation threshold, a high stability was observed, which can be seen in the metrics values on the range of segmentation threshold (Fig. 2).

An example of successful MF detection and segmentation process is illustrated in Fig. 3, which demonstrated the original panoramic x-ray image (Fig. 3(a)) with corresponding detection and segmentation of the MF by neural network (Fig. 3(b)). In some cases, the successful operation of the algorithm was accompanied by additional false positive detections, as observed in Fig. 4(b), or partial or complete lack of detection of the observable MF on the panoramic image as illustrated in Fig. 5(b).

Table 1: Results of mandibular foramen (MF) segmentation

Type of network	DSC	Precision	Recall	$M_{FTP}R$	MF_{FPR}
Single network α = 0.5	47.43	71.13	51.95	76.69	14.08
Single network α = 0.1	49.51	52.26	67.08	84.06	19.01
Single network α = 0.01	48.78	45.23	68.24	87.81	21.35
Cascade of networks	31.77	23.92	88.83	93.75	46.1

DSC–Dice similarity coefficient; MF_{TPR}–MF-wise true positive rate; MF_{FPR}–MF-wise false positive rate

DISCUSSION

In this study, MF was chosen as an anatomical formation of a certain clinical importance. In clinical practice, incorrect detection of structures like the MF might end in significant complications. This study has tested the possibility of automatic detection and segmentation of MF by means of a neural network. In medicine in general, and in dentistry in particular, due to the difficulty in preparing a large dataset, we decided to focus on a small dataset and use a proper neural network architecture as the U-net. U-net has been originally created for use in biomedical research and has proven its effectiveness in small datasets [31, 36]. In this study, only 112 panoramic X-ray images were used, however the number of samples was significantly increased due to augmentation. It is important to note that the U-network has demonstrated a high degree of detection and stability to changes in the threshold value, as shown by the example of the first single network (Fig.2), and this trend was evident in all experiments, including the cascade of networks. The cascade of networks has shown better results than single networks in recall and MF_{TPR}. A good level of recalls (88.83%) and MF_{TPR} (93.75%) was obtained, indicating the high detection capability of the network. Conversely, there has been a significant increase in the false positive results (Fig. 4). A high degree of detection will allow to minimize false negative results, however in the present configuration, the network was accompanied by a very high percent of false positive results (MF_{FPR}=46.1%). In the case of anatomical structures like the MF, the process of differential diagnosis is not likely to cause significant problems for the clinicians, but in the case of various abnormalities it might lead to significant complications.

The minimum criterion for determining detection and segmentation as a positive result was the capturing of eight pixels of MF by the trained network. As shown in Figs. 3 and 4, the detection outcome was quite accurate, but the similarity was insufficient, which was expressed by a moderate DSC, which has reached a maximum value of 49.51% in single network. The present DSC values were similar to the findings of another study in the dental area [36]. Changes in the Tversky index had almost no effect on the DSC and paradoxically the minimum DSC values were in the cascade of networks. Practically, the incomplete correlation between the automatically received segmentation and the true MF can make it difficult for specialists

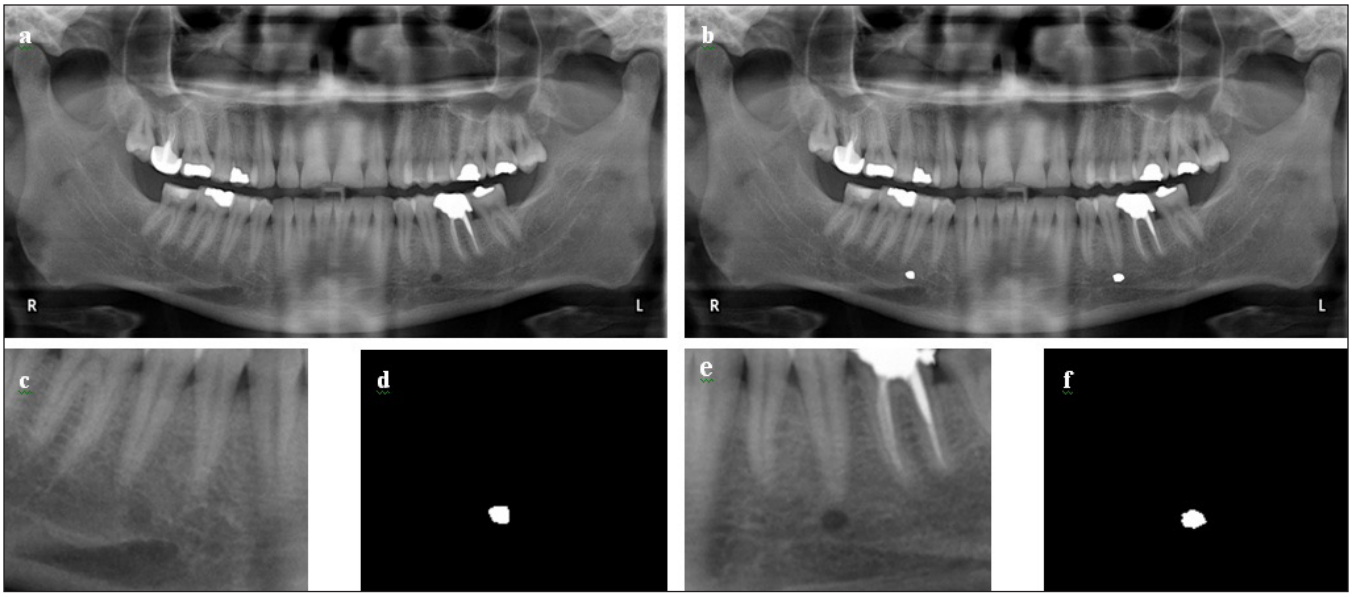

Figure 1: Segmentation of MF. Original digital Panoramic X-ray image (a) and corresponding manual segmentation of the MF (b). Automatically cropped left (c) and right (e) region of interest (ROI) and generated segmentation mask (white: segmented MF, black: background) (d, f).

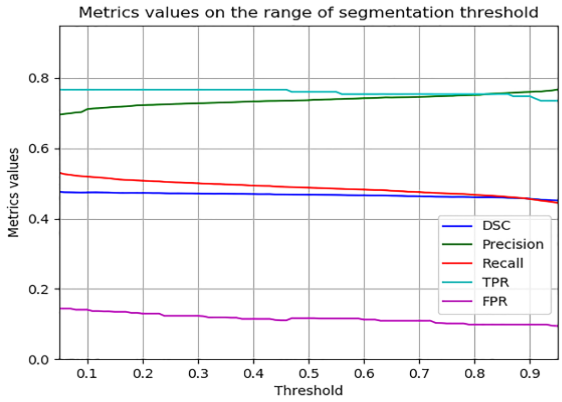

Figure 2: Metrics values on the range of segmentation threshold.

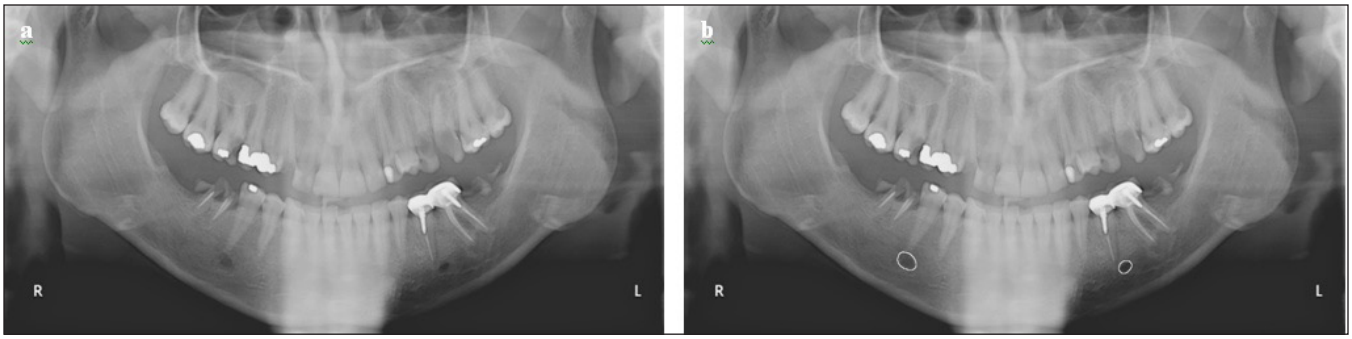

Figure 3: An example of successful MF detection and segmentation process. Original panoramic X-ray image (a) with corresponding detection and segmentation of the MF by neural network (b).

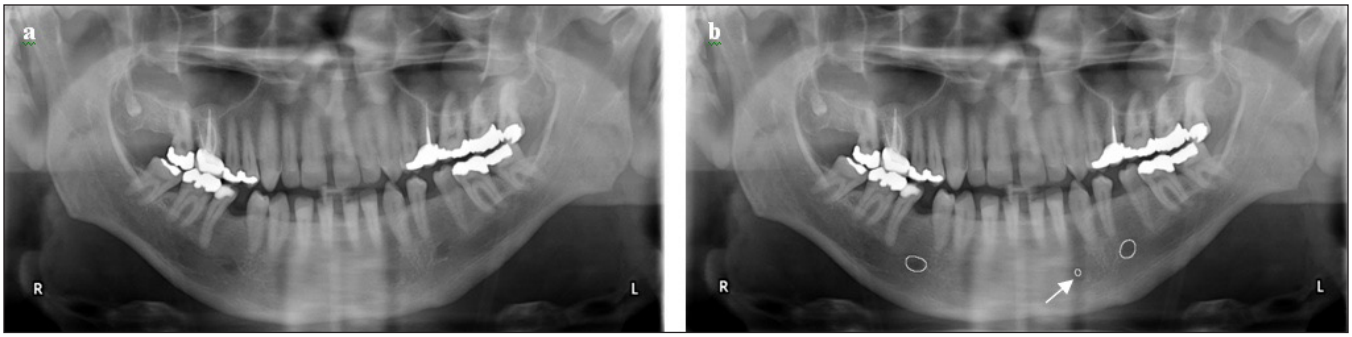

Figure 4: An example of successful detection and segmentation process accompanied by a problematic false positive result. (a) Original digital panoramic X-ray image. (b) The successful operation of the algorithm was accompanied by additional false positive detection (arrow).

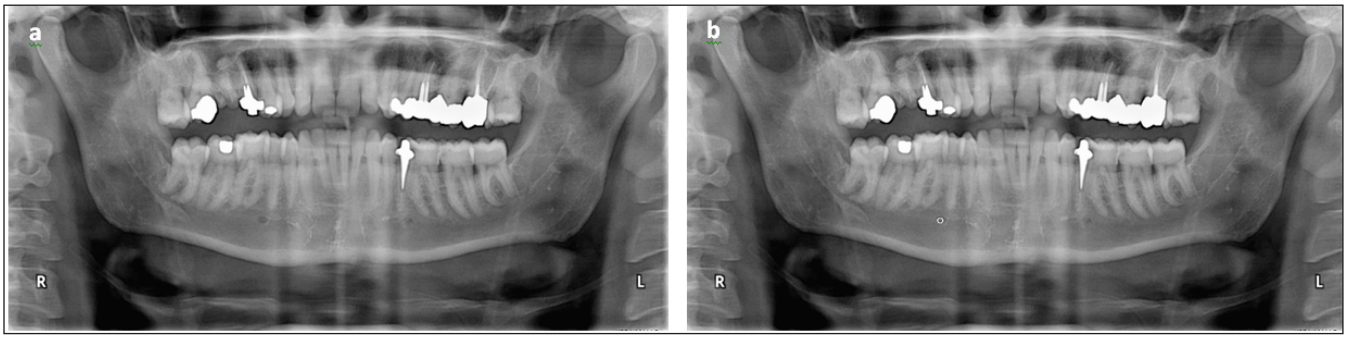

Figure 5: An example of partial detection. (a) Original digital panoramic X-ray image. (b) Complete lack of detection of the observable MF on the left side of the panoramic image.

to detect boundaries, but it is necessary to take into consideration the blurring of MF boundaries on two-dimensional images. In general, the overlapping of all anatomical structures at this location, resulting in blurred boundaries, may explain the low DSC values achieved in our study.

As it is known, X-rays are a poorly balanced form of data, where the anatomical or pathological formation required to be detected, constitutes a small part of all the digital image data. The use of the Tversky index [35, 37] made it possible to compensate for the imbalance of the data and to tune the balance between precision and recall. As expected, this resulted in an increase in recall from the minimum value of 51.95% to 88.83% and a decrease in precision from maximum value 71.13% to 23.92%. Therefore, the use of the Tversky index is important in studies that aim to detect a certain pathology or anatomical structure, and the reduction of false negative results (i.e., missed task objects) is of crucial importance in the clinical setting. In this study, a relatively high level of MF detection and segmentation was achieved using the mentioned methods, although the maximum level of detection was accompanied by an increase in the false positive results and a decrease in DSC. Currently, as a result of the small number of studies in the field of deep learning in maxillofacial radiology [38], there is no possibility to compare our results to those of other similar studies. In addition, there are no well-established standardization schemes to allow accurate and valid comparisons. However, the results of this study and those of a previous research [38] may serve as a platform for perspective research in this field.

CONCLUSIONS

Detection and segmentation of anatomical and pathological structures on X-rays is of great importance. Computer-aided detection systems based on various techniques, mainly deep learning, have demonstrated their effectiveness in performing computer-aided radiology tasks. The developed algorithms on the basis of deep learning for biomedical application have been shown to be highly efficient. Currently, one of the most used neural network architecture for this purpose is the U-net, which was effectively used in this study. The application of additional functions, such as the Tversky index and neural network combination systems, as a cascade of neural networks leads to a significant improvement in the detection capability of the model. The growing number of X-ray scans and the incredibly rapid increase in the number of medical information in the absence of expertized medical staff, especially in developing countries, make methods based on automatic detection, segmentation and classification extremely important and require further development.

REFERENCES

1. Laher AE, Wells M, Motara F, Kramer E, Moolla M, Mahomed Z. Finding the mental foramen. Surg Radiol Anat 38: 469-76, 2016.
2. Smith MH, Lung KE. Nerve injuries after dental injection: a review of the literature. J Can Dent Assoc 72: 559-564, 2006.
3. Greenstein G, Tarnow D. The mental foramen and nerve: clinical and anatomical factors related to dental implant placement: a literature review. J Periodontol 77: 1933-43, 2006.
4. Chong BS, Gohil K, Pawar R, Makdissi J. Anatomical relationship between mental foramen, mandibular teeth and risk of nerve injury with endodontic treatment. Clin Oral Investig 21: 381-7, 2017.
5. Laher AE, Wells M, Motara F, Kramer E, Moolla M, Mahomed Z. Finding the mental foramen. Surg Radiol Anat 38: 469-76, 2016.
6. Iwanaga J, Watanabe K, Saga T, Tabira Y, Kitashima S, Kusukawa J, Yamaki K. Accessory mental foramina and nerves: application to periodontal, periapical, and implant surgery. Clin Anat 29: 493–501, 2016.
7. Borghesi A, Pezzotti S, Nocivelli G, Maroldi R. Five mental foramina in the same mandible: CBCT findings of an unusual anatomical variant. Surg Radiol Anat 40: 635-40, 2018.
8. Rahpeyma A, Khajehahmadi S. Accessory Mental Foramen and Maxillofacial Surgery. J Craniofac Surg 29: 216-7, 2018.
9. Muinelo-Lorenzo J, Suárez-Quintanilla JA, Fernández-Alonso A, Varela-Mallou J, Suárez-Cunqueiro MM. Anatomical characteristics and visibility of mental foramen and accessory mental foramen: Panoramic radiography vs. cone beam CT. Med Oral Patol Oral Cir Bucal 20: 707-14, 2015.
10. Moro A, Abe S, Yokomizo N, Kobayashi Y, Ono T, Takeda T. Topographical distribution of neurovascular canals and foramens in the mandible: avoiding complications resulting from their injury during oral surgical procedures. Heliyon 4: 00812, 2018.
11. Charron O, Lallement A, Jarnet D, Noblet V, Clavier JB, Meyer P. Automatic detection and segmentation of brain metastases on multimodal MR images with a deep convolutional neural network. Comput Biol Med 95: 43–54, 2018.
12. van Ginneken B. Fifty years of computer analysis in chest imaging: rule-based, machine learning, deep learning. Radiol Phys Technol 10: 23-32, 2017.
13. Kooi T, Litjens G, van Ginneken B, Gubern-Mérida A, Sánchez CI, Mann R, den Heeten A, Karssemeijer N. Large scale deep learning for computer aided detection of mammographic lesions. Med Image Anal 35: 303-12, 2017.
14. Zhang, K., Wu, J., Chen, H. & Lyu, P. An effective teeth recognition method using label tree with cascade network structure. Computerized Medical Imaging and Graphics 68: 61–70, 2018.
15. Miki Y, Muramatsu C, Hayashi T, Zhou X, Hara T, Katsumata A, et al. Classification of teeth in cone-beam CT using deep convolutional neural network. Comput Biol Med 80: 24–9, 2017.
16. Chen H, Zhang K, Lyu P, Li H, Zhang L, Wu J, Lee CH. A deep learning approach to automatic teeth detection and numbering based on object detectionin dental periapical films. Sci Rep doi: 10.1038/s41598-019-40414-y, 2019.
17. Tuzoff DV, Tuzova LN, Bornstein MM, Krasnov AS, Kharchenko MA, Nikolenko SI, Sveshnikov MM, Bednenko GB. Tooth detection and numbering in panoramic radiographs using convolutional neural networks. Dentomaxillofac Radiol doi:10.1259/dmfr.20180051, 2019.
18. Lee JH, Kim DH, Jeong SN, Choi SH. Detection and diagnosis of dental caries using a deep learning-based convolutional neural network algorithm. J Dent 77: 106-11, 2018.
19. Lee JH, Kim DH, Jeong SN, Choi SH. Diagnosis and prediction of periodontally compromised teeth using a deep learning-based convolutional neural network algorithm. J Periodontal Implant Sci 48: 114–23, 2018.
20. Krois J, Ekert T, Meinhold L, Golla T, Kharbot B, Wittemeier A, Dörfer C, Schwendicke F. Deep Learning for the Radiographic Detection of Periodontal Bone Loss. Sci Rep doi: 10.1038/s41598-019-44839-3, 2019.
21. Lee JS, Adhikari S, Liu L, Jeong HG, Kim H, Yoon SJ. Osteoporosis detection in panoramic radiographs using a deep convolutional neural network-based computer-assisted diagnosis system: a preliminary study. Dentomaxillofac Radiol 13: 20170344, 2018.
22. Kats L, Vered M, Zlotogorski-Hurvitz A, Harpaz I. Atherosclerotic carotid plaque on panoramic radiographs: neural network detection. Int J Comput Dent 22: 163-9, 2019.
23. Kim DW, Kim H, Nam W, Kim HJ, Cha IH. Machine learning to predict the occurrence of bisphosphonate-related osteonecrosis of the jaw associated with dental extraction: A preliminary Report Bone 116: 207-14, 2018.
24. Murata M, Ariji Y, Ohashi Y, Kawai T, Fukuda M, Funakoshi T, Kise Y, Nozawa M, Katsumata A, Fujita H, Ariji E. Deep-learning classification using convolutional neural network for evaluation of maxillary sinusitis on panoramic radiography. Oral Radiol 35: 301-7, 2019.
25. Ribera NT, de Dumast P, Yatabe M, Ruellas A, Ioshida M, Paniagua B, Styner M, Gonçalves JR, Bianchi J, Cevidanes L, Prieto JC. Shape variation analyzer: a classifier for temporomandibular joint damaged by osteoarthritis. Proc SPIE Int Soc Opt Eng doi: 10.1117/12.2506018, 2019.
26. de Dumast P, Mirabel C, Cevidanes L, Ruellas A, Yatabe M, Ioshida M, Ribera NT, Michoud L, Gomes L, Huang C, Zhu H, Muniz L, Shoukri B, Paniagua B, Styner M, Pieper S, Budin F, Vimort J-B, Pascal L, et al. A web-based system for neural network based classification in temporomandibular joint osteoarthritis. Comput Med Imaging Graph 67:45–54, 2018.
27. Ekert T, Krois J, Meinhold L, Elhennawy K, Emara R, Golla T, Schwendicke F. Deep Learning for the Radiographic Detection of Apical Lesions J Endod 45: 917-22, 2019.
28. Ariji Y, Yanashita Y, Kutsuna S, Muramatsu C, Fukuda M, Kise Y, Nozawa M, Kuwada C, Fujita H, Katsumata A, Ariji E. Automatic detection and classification of radiolucent lesions in the mandible on panoramic radiographs using a deep learning object detection technique. Oral Surg Oral Med Oral Pathol Oral Radiol 128: 424-30, 2019.
29. Poedjiastoeti W, Suebnukarn S. Application of Convolutional Neural Network in the Diagnosis of Jaw Tumors. Health Inform Res 24: 236-41, 2018.
30. Ariji Y, Sugita Y, Nagao T, Nakayama A, Fukuda M, Kise Y, Nozawa M, Nishiyama M, Katumata A, Ariji E. CT evaluation of extranodal extension of cervical lymph node metastases in patients with oral squamous cell carcinoma using deep learning classification. Oral Radiol doi: 10.1007/s11282-019-00391-4, 2019.
31. Ronneberger O, Fischer P, Brox T. (2015) U-Net: Convolutional Networks for Biomedical Image Segmentation. In: Navab N., Hornegger J., Wells W., Frangi A. (eds) Medical Image Computing and Computer-Assisted Intervention – MICCAI 2015. Lecture Notes in Computer Science, vol 9351. Springer, Cham. MICCAI 2015.
32. Brosch T, Tang LY, Youngjin Yoo, Li DK, Traboulsee A, Tam R. Deep 3D Convolutional Encoder Networks With Shortcuts for Multiscale Feature Integration Applied to Multiple Sclerosis Lesion Segmentation. IEEE Trans Med Imaging 35: 1229-39, 2016.
33. Nair V, Hinton G. ICML'10. Proceedings of the 27th International Conference on International Conference on Machine Learning; 2010 June 21–24; Haifa, Israel. USA: Omnipress; p.807-14, 2010.
34. Dice L. Measures of the Amount of Ecologic Association Between Species. Ecology. 1945; 26: 297-302.
35. Tversky A. Features of similarity. Psychol Rev 84: 327-52, 1977.
36. Ronneberger O, Fischer F, Brox T. Dental X-ray Image Segmenation using a U-shaped Deep Convolutional Network. https://arxiv.org/abs/1505.04597, 2015.
37. Salehi SS, Erdogmus D, & Gholipour A. Tversky loss function for image segmentation using 3D fully convolutional deep networks. Tversky as a Loss Function for Highly Unbalanced Image Segmentation using 3D Fully Convolutional Deep Networks. https://arxiv.org/abs/1706.05721, 2017.
38. Hwang JJ, Jung YH, Cho BH, Heo MS. An overview of deep learning in the field of dentistry. Imaging Sci Dent 49: 1-7, 2019.